Reaction Chemistry & Engineering

ROYAL SOCIETY OF CHEMISTRY

PAPER

View Article Online
View Journal | View Issue



Cite this: *React. Chem. Eng.*, 2026, 11, 306

# General approach for automated purification of quantum dots using size-exclusion chromatography

Rui Hua Jeff Xu, [a] Conan Huang,[b] Logan P. Keating, [b] Yunpei Duan, [b] Moonsub Shim [b] and Paul J. A. Kenis *[a]

Colloidal semiconductor nanocrystals or quantum dots (QDs) are a class of materials with size and shape-dependent optoelectronic properties that show potential for a range of applications. Discovery of new QDs with interesting properties and optimization of their synthesis require a rapid, generalizable, and scalable purification method to separate QDs from reaction mixtures. This paper describes a size-exclusion chromatography (SEC)-based approach that enables rapid, efficient separation of QDs from crude QD reaction mixtures. Using commercially available C-18 capped silica columns and off-the-shelf components, we report an automated liquid-chromatography platform with integrated optical characterization (UV-vis) for in-line optical characterization. This platform was used to investigate the effects of column operating parameters on QD separation performance and was further validated using six crude QD samples of different sizes, shapes, and compositions. Ligand coverage of the purified QD fractions can be tuned by controlling column parameters, with higher temperatures and residence times leading to ligand shedding of QDs. NMR analysis of purified QDs showed reduced solvent and ligand impurities when compared to samples purified using a precipitation–redissolution method. This SEC method provides a rapid (<2 min) approach for one-step purification of crude QDs on analytical or preparative scales and can be seamlessly integrated into existing QD or other nanocrystal research workflows.

Received 11th July 2025,
Accepted 15th October 2025

DOI: 10.1039/d5re00302d

rsc.li/reaction-engineering



## Introduction

Colloidal quantum dots (QDs) are a promising class of materials with applications in bioimaging, photocatalysis, sensors, photodetectors and solar cells, luminescent solar concentrators (LSCs), displays, and LEDs, lasers, and other applications.[1–19] Presently, most QDs are synthesized using high-temperature (>200 °C) solution-phase synthesis in high boiling point organic solvents (*e.g.*, octadecene, trioctylphosphine oxide, and squalane) with precursors and surface-passivating ligands consisting of a mixture of cation, anion, and organic reagents to stabilize particles in solution and to ensure an electronically passivated and inert surface.[7,20–23] These methods generate QDs capped with various ligands suspended in reaction mixtures that contain nonvolatile solvent(s), excess coordinating ligands, unreacted precursors, and reaction products/byproducts.[24–28] QD applications require purification to remove nanoparticles from other species in as-synthesized crude reaction mixtures.[29] For example, device fabrication requires pure QDs at high concentrations without dissolved organic impurities to achieve high quality, homogeneous films with excellent QD interparticle packing.[30,31] Purification prior to heterostructure growth can also help improve shell growth and/or ligand exchange required for various QD applications.[27,28,32,33] Besides being essential for QD applications, QD purification is important for many structural and chemical characterization methods that require clean QDs (*e.g.*, (S)TEM, ICP-MS), or QDs that are concentrated and deposited (*e.g.*, XRD) – or direct imaging *via* electron microscopy of QDs.[34] Imaging poorly purified QDs can result in *in situ* electron beam reactions, and deposition of carbon moieties within the imaging environment.[35,36] Thus, purification of QDs is critical for both characterization and further downstream applications.

Current purification methods for QDs largely can be grouped into three approaches: solubility-based, electrophysical, and size-based, as recently summarized by Kim *et al.* in a comprehensive review.[37] Solubility-based methods rely on the differences in solubility of QDs *vis-à-vis* the solubility of dissolved impurities. These methods include the commonly used precipitation and redissolution (PR) method that involves flocculation of QDs by adding an antisolvent to a nonpolar phase and centrifuging the resulting mixture to separate the

[a] *Department of Chemical and Biomolecular Engineering, University of Illinois Urbana Champaign, Urbana, IL, 61801, USA. E-mail: kenis@illinois.edu*
[b] *Department of Material Science & Engineering, University of Illinois Urbana Champaign Urbana, IL, 61801, USA*

flocculated QDs from the dissolved impurities.[29,32,38–40] The precipitated QDs can then be redispersed into a desired solvent and the PR step can be repeated several times to ensure impurities are sufficiently removed. Electrophysical methods such as electrophoresis, on the other hand, rely on the deposition of QD particles on a solid electrode when exposed to an electric field, while size-based methods such as size-exclusion chromatography (SEC) rely on the size differences between QDs and impurity molecules. While these methods can purify QDs at high yield, they all possess various disadvantages such as modifying the surface properties of QDs (PR and electrophoretic deposition), high complexity of workflows, lack of generalizable protocols (PR), and low throughput (SEC).

Among the various QD purification methods, SEC has shown to be a promising, nondestructive method for QD purification. SEC works by the difference in the excluded volume (or accessible volume) of larger QD particles (often $>5000$ g mol$^{-1}$) and smaller impurity molecules ($<1000$ g mol$^{-1}$). Larger particles with greater excluded volumes get eluted earlier from SEC columns and can thus be separated from smaller impurity molecules. Recently, several works have demonstrated SEC purification of different QD compositions dissolved in various solvents.[32,34,41–51] Because SEC relies purely on size differences between nanocrystals and other solute molecules in solution, it is highly generalizable – particles, regardless of size, shapes, and compositions, can be separated from the reaction mixture as long as a mobile phase capable of dispersing the particles and dissolving the reactant byproducts/unreacted solute molecules is used, and the particles themselves do not interact with the stationary phase media. It is also a highly scalable method that has been well established for the separation of biomolecules.[52] However, most demonstrated workflows for SEC purification of QDs are relatively time and labor intensive. Currently, SEC has been demonstrated on crosslinked polystyrene-based (PS) gel beads for QD purification and ligand exchange.[32,44] This method can generate highly pure QD particles free from solvent and free ligand impurities but has some notable disadvantages: PS beads swell differently under different solvents and deform under high flowrates, that limits the types of solvents that can be used for QD purification and the maximum separation throughput.

In this paper, we demonstrate an automated method to purify QDs from crude reaction mixtures containing a variety of organic and inorganic impurities. We integrated commercially available components and software to create a modular, automated LC UV-vis platform for SEC purification. The separation performance of our automated SEC platform was characterized by investigating the effects of operation parameters such as flow rates, column temperatures, and column loadings. We then validated this platform using samples from a range of different synthesis chemistries covering a range of QD materials (composition, shape, size, surface ligands). Purified QD samples exhibit high purity based on deep-UV, NMR, and TEM characterization. This demonstrates the potential for integrating the platform with existing automated nanomaterial synthesis platforms to enable more data-rich integrated synthesis and characterization workflows.

# Experimental

### Size-exclusion chromatography platform

Pre-packed analytical C-18 silica columns (Macherey-Nagel EC Nucleosil 100 Å, 7 μm, 125 × 4.6 mm, P/N: 720951.46; Thermo Acclaim 120 Å, 5 μm, 100 × 4.6 mm, P/N: 059147; and Waters Sunfire 100 Å, 5 μm, 100 × 4.6 mm, P/N: 186002558) were purchased and first cleaned by flushing 5 column volumes (c.v.) of 2-propanol (Fisher, HPLC grade) followed by 5 c.v. of hexanes (Fisher CHROMASOLV™ for HPLC, ≥98.5%) at 1μL s$^{-1}$ flowrates. These columns were connected to other components using IDEX connectors and LabSmith CapTite connectors (see Fig. S1). The flow of mobile phase was achieved using Harvard Instruments 70-2220 and 70-2226 syringe pumps and Hamilton gastight glass syringes (P/N: 81320, 81420). Microfluidic valves (LabSmith AV201-T132, AV303-T132) were used to control the flow of sample and mobile phase and for collection of column fractions while a temperature controller (Omega CSI32K-C24) was used to manually control the temperature of the column. An Ocean Optics Flame-S-UV-VIS-ES spectrometer (185–850 nm) connected to an Ocean-Optics DH-mini light source and a Cytiva 2 mm path length flow cell was used for UV-vis absorption spectroscopy. The above equipment was powered using a Mean Well QP-320D DC power supply with 12 V and 24 V power outputs.

### Chemicals for Column Testing

Chemicals used for testing the column were obtained as follows: oleic acid (OA, 98%, Ambeed), trioctylphosphine (TOP, 99%, Chem Impex), squalane (96%, Sigma), octadecene (ODE, 90%, Sigma), oleylamine (OAm, 90% Sigma) are liquids that were diluted 1 : 1 with hexanes (Fisher CHROMASOLV™ for HPLC, ≥98.5%) to create a solutions for testing precursor elution times on the SEC column. Stearic acid (SA, 99%, Sigma) and trioctylphosphine oxide (TOPO, 99%, Sigma) were dissolved into hexanes to form a 20 mM solution for column elution time testing. Cadmium oleate was synthesized by the reaction of cadmium oxide (99.5%, Sigma), with three molar equivalents of oleic acid (98%, Ambeed) in squalane (96%, Sigma) at 200 °C while under a vacuum (to remove water byproduct) to first generate a 300 mM $Cd(OA)_2$ solution, before diluting the solution to 20 mM in hexanes. Trioctylphosphine selenide was synthesized by sonicating selenium (99.95%, Sigma) with 1.2 molar equivalents of trioctylphosphine (99.6%, Chem Impex) to first yield a clear solution, before diluting this solution to 50 mM in hexanes.

### Platform control and operation

All experiments were ran using hexanes (Fisher CHROMASOLV™ for HPLC, ≥98.5%) as the mobile phase and automated using Python. Respective packages from vendors

(Labsmith, LabJack, Ocean Optics) were used to develop code for automating sample loading, mobile phase flow, UV-vis characterization, and fraction collection of the SEC column outputs. Detailed information of the various Python packages used is listed in section S2. Code for operation of the hardware is shared publicly on GitHub: https://github.com/AutonomousWorkflows/SEC_Automation.

### Quantum dot synthesis

Various II–VI QDs of different compositions, particle sizes, and surface ligands were synthesized using methods listed in section S1. The specific compositions, sizes, surface ligands, and chemical compositions of the various samples tested are listed in Table 1 below. All samples were used either as a crude reaction mixture or diluted using toluene (99%, Sigma) to prevent solid precursors (*e.g.*, TOPO, stearic acid) from precipitating out of the reaction mixture. The QD concentration of these samples varied between 0.2 wt% and 2 wt%. All samples were filtered through a 0.45 μm PTFE syringe filter before loading into glass syringes for SEC purification.

### Precipitation–redissolution purification

Per typical precipitation/redissolution methods, a 1 mL aliquot of raw reaction mixture was mixed with 1.5 mL of toluene. 2 mL of ethanol was added, rendering the solution turbid. The test tube was then centrifuged for 5 minutes at 2400 RPM and the precipitate was collected, the test tube was flushed with ethanol then dried in vacuum for 1 minute and then redissolved in 600 μL $CDCl_3$ for $^1$H NMR representing the 1PR sample or 1 mL toluene again for additional purification. For an additional purification pass (2PR) 2.5 mL of ethanol was added and centrifuged again for 5 minutes at 2400 RPM. The precipitate was collected, flushed with ethanol, then dried in vacuum for 1 minute before redispersing in CDCl3 for $^1$H NMR or toluene for TEM.

### *Ex situ* sample characterization

QD fractions collected from the SEC purification were dried in a vacuum oven (Being BOV-20) for 45 minutes at room temperature to yield dried purified QDs. These QD samples (>5 mg) were then re-dispersed into 600 μL $CDCl_3$ (Sigma-Aldrich, 99.8 atom% D). $^1$H NMR spectra were recorded at room temperature on a Varian 600 system at 600 MHz (14.09 Tesla), taking 144 acquisitions. Chemical shifts are reported in ppm with the solvent resonance as the internal standard ($CDCl_3$, 7.26 ppm). TEM imaging of purified QDs is achieved by first drying and redispersing purified QDs into toluene before drop-drying samples on copper 300 mesh grids with thin carbon support. TEM images were obtained on a JEOL 2100 at 200 kV.

## Results and discussion

### Automated chromatography system design

We sought to develop an automated size-exclusion chromatography (SEC) purification platform for crude QD samples, with the goal of separating small (>2 nm) QDs from other constituents in synthesis mixtures (*e.g.*, solvents, ligands, unreacted precursors). SEC is a method to separate particles of different sizes based on their accessible volumes. Larger molecules or particles are unable to access the smaller pores in the stationary phase and thus have a lower accessible volume (greater excluded volume), allowing them to be eluted earlier from the column than smaller molecules or particles.[53] To achieve this, we pursued a modular approach connecting various commercially available pre-packed columns, rotary microfluid valves, syringe pumps, HPLC fittings, and optical spectrometry hardware, as shown in Fig. 1. The SEC column was wrapped with a heating jacket connected to an Omega CSI32K-C24 temperature controller for operations at temperatures up to 60 °C. More detailed schematics and images highlighting all the specific parts used in this platform are shown in Fig. S1 and S2. This home-built LC UV-vis system operates by first loading a specified volume of QD sample directly into the SEC column using a syringe pump, followed by flowing of the mobile phase through the column. UV-vis spectra were collected at 200 ms intervals (5 acquisitions per spectra) for wavelengths between 200 and 750 nm. Syringe pump infusion/withdrawal, valve controls, and UV-vis spectra acquisition were all automated using a Python script. More details regarding the operation of the platform on Python are listed in section S2.

To allow for rapid and versatile SEC purification, we selected porous silica media as the stationary phase because inert silica particles allow for a variety of organic solvents to be used as the mobile phase, whereas gel-based polystyrene beads as the stationary phase would swell to different extents with different solvents and temperatures. Silica columns allow for operation at a range of temperatures (<60 °C) and a

**Table 1** Details of the various QD samples tested with the SEC platform. Specific QD compositions, dimensions, surface ligands, and synthesis precursors within the reaction mixtures are described (SA = stearic acid, OA = oleic acid, OAm = oleylamine, TOP = trioctylphosphine, TOPO = trioctylphosphine oxide, ODPA = octadecylphosphonic acid)

| Sample name | Composition | Particle dimensions | Ligands | Composition |
|---|---|---|---|---|
| CdSe-3.5 | CdSe | 3.5 nm dots | SA | Ref. 60 |
| CdSe-2.6 | CdSe | 2.6 nm dots | OA | Refer to section S1 |
| CdSe-8 | CdSe/ZnSe | 10 nm dots | OA, TOP | Refer to section S1 |
| CdSe-12 | CdSe/CdTe/CdSe | 8 nm dots | OA, OAm | Refer to section S1 |
| DHNR | CdSe/ZnSe | 5 × 25 nm dumbbells | OA, TOP | Ref. 61 |
| 2DNR | CdSe/ZnSe | 2 × 20 nm rods | ODPA, TOPO | Ref. 62 |

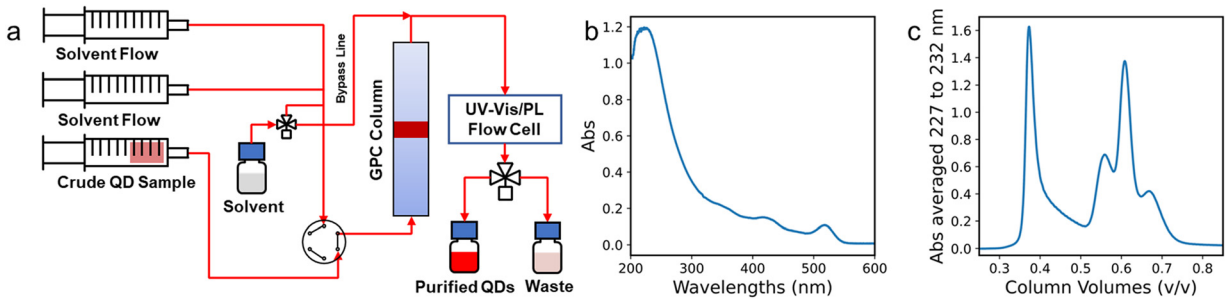


**Fig. 1** (a) Simplified schematic of the SEC LC UV-vis system. (b) Example UV-vis spectra obtained at each timepoint: shown figure is an example of a spectra at an elution time when QDs are present (c) example chromatogram averaged across a specific wavelength range, highlighting the elution peaks of QDs and dissolved organic species.

range of flow rates as rigid silica particles can handle high pressures (<400 bar) and flowrates, whereas gel-based alternatives will deform under high flowrates (<20 bar). More importantly, fully porous silica media also allow for a high degree of size exclusion with a relatively small interstitial volume ($\varepsilon_{interstitial}$ = 0.36–0.42) and relatively large pore volumes ($\varepsilon_{pore}$ = 0.25–0.35). This means that QDs with larger diameters than the pores in silica media will have the largest excluded volume (smallest accessible volume) and exit the column at $\varepsilon_{interstitial}$ × column volume (c.v.) while smaller molecules will have a smaller excluded volume (larger accessible volume) and will exit the column after passing between $\varepsilon_{interstitial}$ and ($\varepsilon_{interstitial}$ + $\varepsilon_{pore}$) × c.v. in volume. This difference in accessible volume allows us to collect the QD fractions that elute early at a high yield. In this work, silica functionalized with a high-coverage of C-18 was used to ensure minimal interaction between components in the crude QD sample (QDs, nonpolar organic precursors) and the column, ensuring that size-exclusion is the main factor in separation. Reverse phase C-18 capped columns were chosen instead of normal phase columns with greater degree of size exclusion as nanoparticles are capped with ligands (carboxylates, phosphonates) that will detach and preferentially adsorb to normal phase columns. This ligand detachment eventually leads to ligand-stripped QD particles adhering to the polar groups on the silica and getting trapped in normal phase columns. Using C-18 capped reverse phase columns with high surface functionalization avoids this issue by creating a nonpolar layer that prevents the particles from adhering to the underlying silica.

### Column testing and performance

In all the experiments listed hereafter, HPLC-grade hexanes was used as the mobile phase as it is highly optically transparent in the deep UV region (UV cutoff ~195 nm). This solvent is also nonpolar and can thus dissolve most of the nonpolar precursors used in QD synthesis at high concentrations. Hexanes is also a low viscosity solvent, allowing for higher flow rates, while being readily available at a low cost. We tested three different kinds of C-18 capped silica between 5 μm and 7 μm, with particle sizes ranging from 100 Å to 120 Å. CdSe-3.5 particles approximately 3.5 nm in mean diameter were used as the test sample. The resulting chromatograms of these three columns are shown in Fig. 2 below.

All columns show distinct QD peaks when viewed at the visible range (solid lines) of the acquired spectra. The Thermo Acclaim 120 Å column demonstrates two distinct narrow QD peaks at 0.54 c.v. and 0.60 c.v., as well as a series of peaks (dotted lines, measured at deep UV wavelengths) corresponding to other organic constituents between 0.55 c.v. and 0.68 c.v. This shows that the small 3 nm particles elute from the Thermo Acclaim 120 Å column, at a value between $\varepsilon_{interstitial}$ (typically ~0.36 c.v.) and $\varepsilon_{interstitial}$ + $\varepsilon_{pore}$, (typically ~0.7 c.v.) suggesting that the particles can enter the larger 120 Å pores in this column's media. Given the dimensions of the capping ligands (22 Å for length of stearic acid), the QDs will have an effective size of about 35 + 22 + 22 = 79 Å, while the pores will have an effective size of 120 − 22 − 22 = 78 Å. The similar pore size of the silica compared to the size of the ligand-capped QD thus allows the ligand to enter the pores and elute at a volume greater than $\varepsilon_{interstitial}$. The second peak at 0.6 c.v., likely corresponds to a smaller population of smaller particles, possibly QDs with a smaller effective diameter from having shed their ligands. The lack of separation between the QD peak (0.54 c.v.) and the other organic peaks (0.55 c.v.) thus makes this column unsuitable for QD purification.

On the other hand, both the Macherey-Nagel (MN) column and the Waters column show elution of QDs at 0.36 and 0.39 c.v. respectively. These two columns show broad peaks that elute later (>0.54 c.v.) in the deep UV (205 to 245 nm) range of the spectra. The rapid elution of QDs in these two columns suggest that most QDs are unable to enter the pores in the silica. Both the Waters and MN columns have 100 Å pores, that corresponds to an effective mean pore size of 100 − 22 − 22 = 56 Å after considering the dimensions of the octadecylsilyl capping. This is sufficient to fully exclude the 3.5 nm CdSe QDs capped with 22 Å stearate ligands (79 Å diameter).

Both the Waters and MN columns also demonstrated broader peaks with significant tailing. This tailing can be attributed to two possible causes: attractive forces between

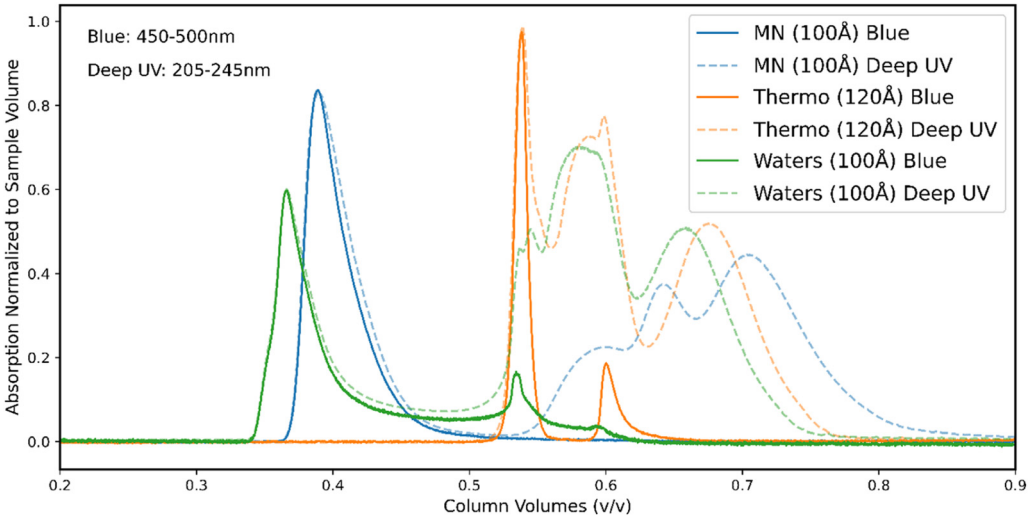


**Fig. 2** Chromatograms of CdSe-3.5 QDs for the tested columns at room temperature. Flow rates of all columns are 0.5 μL $s^{-1}$ with a sample loading of 0.25% × c.v. All solid curves are normalized to injected sample volume. Solid lines show absorption averaged in the blue (450–500 nm) range of the measured spectrum and correspond only to the absorption of QDs. Dotted lines show absorption averaged in the deep UV (205–245 nm) range of the measured spectrum and corresponds to absorption from both QDs and other organic compounds in the samples.

column and QDs, and ligand-shedding of QD particles. Attractive interactions between QD particles and the column stationary phase leads to particle adhesion to the stationary phase, causing an increase in elution times leading to the observed peak tailing. Ligand shedding, on the other hand, is caused by the local equilibrium between bound and free ligands: samples in crude reaction mixture have free ligands around them that can associate or dissociate with the QD surface, while QDs flowing in the column will elute ahead of any free ligands in the crude reaction mixture. This leads to ligand-bound QDs being exposed to ligand-free hexane that drives the ligand dissociation reaction, leading to gradual shedding of bound ligands. Over time, this reduces the effective diameter of QD particles, allowing some particles to enter the pores of the silica and thus elute later from the column. More evidence for these two phenomena will be presented below.

In comparing the MN column and the Waters column, the MN column exhibited less tailing and more efficient separation of QDs from other organic components (MN Deep UV line in Fig. 2). All experiments discussed hereafter were thus be carried out on this column. Detailed calculations for the operating limits of this column are shown in section S3. We then further tested this column by injecting small volumes of single QD synthesis precursors into the reactor. This determines the elution times (in c.v.) of commonly used QD synthesis precursors and allows for determination of the cut-off-points for collecting pure QD fractions. The peak positions of various common precursors are shown in Table 2.

**Effect of operating parameters on column performance.** After determining the suitability of MN column through injection of single precursors and CdSe-3.5 crude QD sample, we then proceeded to systematically investigate the effect of column operating parameters (temperatures, flow rates, column loading) on the separation performance of the SEC system. Firstly, CdSe-3.5 was used to determine the effects of temperature and flowrate on separation performance. Thereafter, the effect of column loading was tested with particles of different sizes and shapes in CdSe-2.6 dots and nanorod heterostructure (DHNR).

### Effect of temperatures and flowrates

The column was tested using CdSe-3.5 to determine the effects of column temperature and column flowrate on separation performance, with the results shown in Fig. 3. In these experiments, the flowrate was varied from 25.6 μL $s^{-1}$ (residence time $\tau$ = 80 s) to 0.2 μL $s^{-1}$ ($\tau$ = 10 300 s). The column was also operated at a low (21 °C) and high (55 °C) temperature to

**Table 2** Peak positions of various commonly used precursors for II–VI QD synthesis. 5 μL of each sample is injected into the column at 55 °C before hexanes are eluted at 5 μL $s^{-1}$ to obtain these elution volumes. Higher temperatures are used to ensure solubility of the heavier organic species in hexane. Note that nanoparticles will elute at <0.42 c.v., while most organic compounds present in reaction mixtures will elute at >0.55 c.v. This enables separation of QDs to a high purity

| Compound | MW | Elution volume (c.v.) |
|---|---|---|
| QDs (>2 nm) | >2000 | 0.35–0.42 |
| Squalane | 422.8 | 0.60 |
| Octadecene | 252.5 | 0.61 |
| Oleylamine | 267.5 | 0.60 |
| Stearic acid | 284.5 | 0.71 |
| Oleic acid | 282.5 | 0.72 |
| Cadmium oleate | 675.3 | 0.59 |
| Trioctylphosphine | 370.6 | 0.64 |
| Trioctylphosphine selenide | 449.6 | 0.73 |
| Trioctylphosphine oxide | 386.7 | 0.72 |
| Toluene | 92.14 | 0.68 |

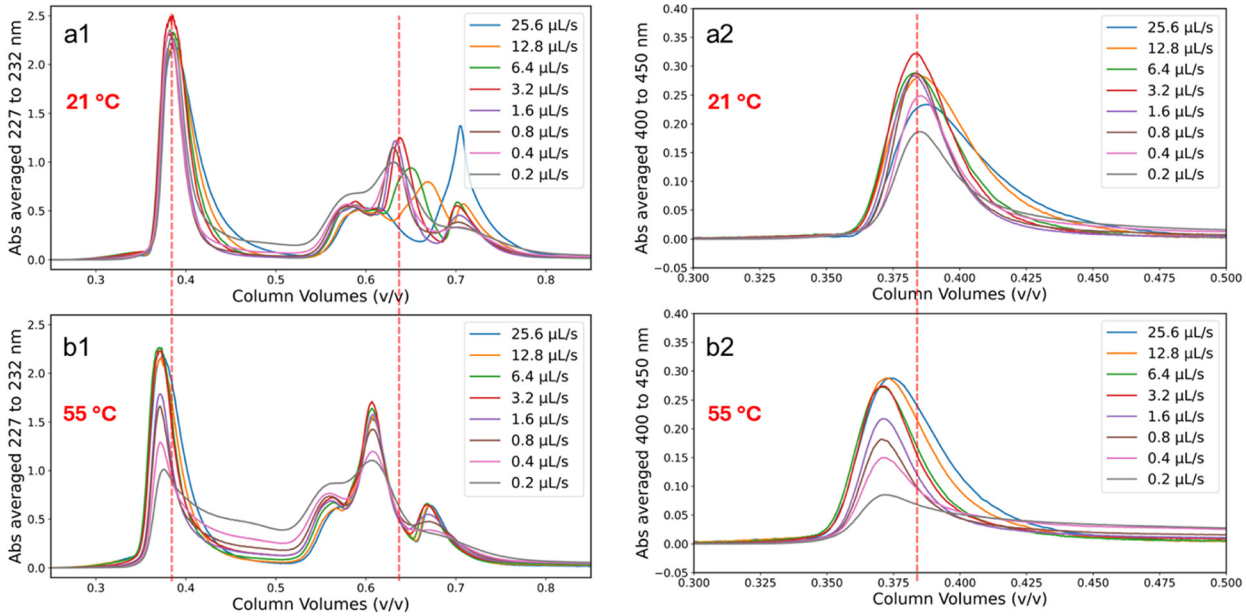


Fig. 3 Chromatograms of CdSe-3.5 QDs at various flow rates and temperatures. (a1) Chromatogram at 227 to 232 nm, a window deliberately chosen to avoid the absorption peaks of toluene, while ensuring the absorbance of other present organic compounds is sufficiently low. (a2) Chromatogram when averaged from 400 to 450 nm, a window that shows only the absorption of QDs. (b1) and (b2) same as (a1) and (a2) but with the column heated to 55 °C. All experiments were carried out with 5 µL (0.25% c.v.) of crude CdSe-3.5 QD sample.

determine the effect of temperature on separation performance. These temperatures were chosen based on the temperature limit (60 °C) of the column. High temperature operation of the column is important as it can ensure greater reliability – it increases the solubility of some heavier nonpolar organic compounds found in QD synthesis (*e.g.*, stearic acid, TOPO) and ensures that these compounds do not precipitate while they are flowing through the column.

### Discussion of peak positions

Fig. 3a1 and b1 shows the chromatograms of CdSe-3.5 at various flowrates at low and high temperatures respectively. These chromatograms were measured at wavelengths between 227 and 232 nm, corresponding to a minimum in the absorption spectrum of toluene (that was used to prepare the sample). In these chromatograms, we can see the elution of the QD peak at 0.39 c.v. (21 °C) and 0.37 c.v. (55 °C) respectively. This result shows that the QDs cannot access the pores in the silica and thus elute early at $\varepsilon_{\text{interstitial}}$. On the other hand, the dissolved organic species in the crude reaction mixture elute at between 0.55 c.v. and 0.7 c.v., showing their ability to access a greater volume of the silica since they can fit into the silica pores. This large difference in the peak positions between QDs (<0.4 c.v.) and organic species (>0.55 c.v.) thus allows separation of QDs at high purity.

### Effect of temperature

One other observation from Fig. 3 is that for both the QD peaks and organic peaks, increasing the temperature from 21 to 55 °C leads to a more rapid elution of all species without any change in the relative positions of the peaks. This is mainly due to the lower density of the mobile phase at higher temperatures. Organic solvents such as hexanes have significant density changes with temperature. An increase in temperature from 21 °C to 55 °C leads to an approximately 5% decrease in fluid density – the expansion of the mobile phase as it is injected from a room-temperature syringe into a 55 °C column thus leads to shorter elution time for all species. Temperature does not seem to influence the relative peak positions of the QD and organic peaks, suggesting that size-exclusion is the main driving force of separation.

### Effect of flow rates

At both high (55 °C) and low (21 °C) temperature, we also observe changes in the peak width of the QD peak (Fig. 3a2 and b2). Specifically, we observe differences in peak tailing at different flow rates. Generally, as flow rates decrease from 25.6 to 1.6 µL $s^{-1}$, the peak width decreases. This decrease in peaks with decreasing flow rates can be attributed to mass transfer limitations. Increased flowrates lead to restricted diffusion and irregular flow patterns, leading to broad and tailing peaks.[54] At higher flowrates (lower residence times), some QD particles do not have adequate time to diffuse out of the small spaces between silica particles and this leads to some QD particles eluting later. In essence, the separation is poorer (wider peaks) due to mass transfer limitations. This issue can however be partially mitigated by operating the column at higher

temperatures to increase mass transfer when operating at high flow rates (Fig. 3b2).

### Peak tailing due to ligand shedding

However, as flow rates are further reduced from 1.6 ($\tau$ = 1289 s) to 0.2 μL $s^{-1}$ ($\tau$ = 10 300 s), we can see a pronounced increase in peak tailing (Fig. 3a2 and b2). This effect is also more pronounced at higher temperatures, with the peaks at 51 °C showing significantly more tailing. This suggests that this tailing effect is both residence time and temperature dependent, with longer residence times and higher temperatures contributing to more tailing. As ligand-capped QDs travel through the column, they gradually shed ligands, leading to smaller effective diameters. Eventually, some of these QDs will be able to access the pores in the silica and/or adhere to the silica and thus elute later from the column.

Overall, both temperature and flow rate playing a significant role in the separation performance of SEC with silica media is evidenced. Changing temperature and column residence time can greatly affect the number of ligands shed by QD particles as they pass through the column. Column operation at lower temperatures and shorter residence times will generate QDs with more surface ligands conserved, while column operation at higher temperatures and longer residence times will generate QD fractions with more ligand-shed surfaces. Generally, QDs with more surface ligands are preferred for handling, as the presence of ligands at higher densities on QD surfaces leads to lower probability of QD agglomeration. These QDs are also more processable, able to be easily dried and re-dispersed into other solvents for characterization or various downstream applications such as device fabrication. Because the goal is to generate QDs that are more solution processible for characterization studies, the rest of the experiments in this paper focus on QDs separated at high flow rates at room temperature.

### Effect of sample loading (volumes)

To investigate the loading capacity of the column, we tested the effect of column loading on separation performance. We injected various sample volumes of DHNRs into the column (0.25% to 3% c.v.) with the resulting chromatogram shown in Fig. 4a1. The width and position of the QD peak did not change with column loading up to 3% of the column loading, as detailed in the chromatogram shown in Fig. 4a2. This suggests that size exclusion is the main driving force of separation in our platform and this column is capable of rapid separation at high column loadings.

However, at higher particle concentrations (*e.g.*, by using more concentrated crude reaction mixtures), there appears to be a change in shape of the QD peak as column loading increases (Fig. 4b). At higher column loadings of 2.6 nm CdSe there appears to be a secondary peak/shoulder forming. This suggests that the tailing is QD-concentration dependent, likely due to the QD interactions with the stationary phase. At higher QD concentrations, QDs can adhere to the stationary phase leading to tailing in the chromatograms. Such tailing will not affect the separation purity of QDs but will decrease its yield due to some QDs eluting the column past the cutoff volumes.

Overall, by varying operating parameters of this column, we demonstrated that C-18 modified fully porous silica particles are suitable for rapid purification of QDs from the heavy nonpolar organic phases used in high temperature colloidal synthesis. This approach enables rapid, one-step purification of QDs at relatively high (3% c.v.) column loadings. Purification performance, however, depends on operating parameters such as temperatures, flow rates, and QD concentrations. QD particles can shed ligands as they pass through the column, so shorter residence times (high flow rates) and lower temperatures can help conserve ligands on purified QDs. In fact, QDs purified at high temperatures and low flow rates often lead to particles that are difficult to redisperse after drying compared to QDs purified at lower temperatures and high flowrates due to this phenomenon. This ligand shedding can

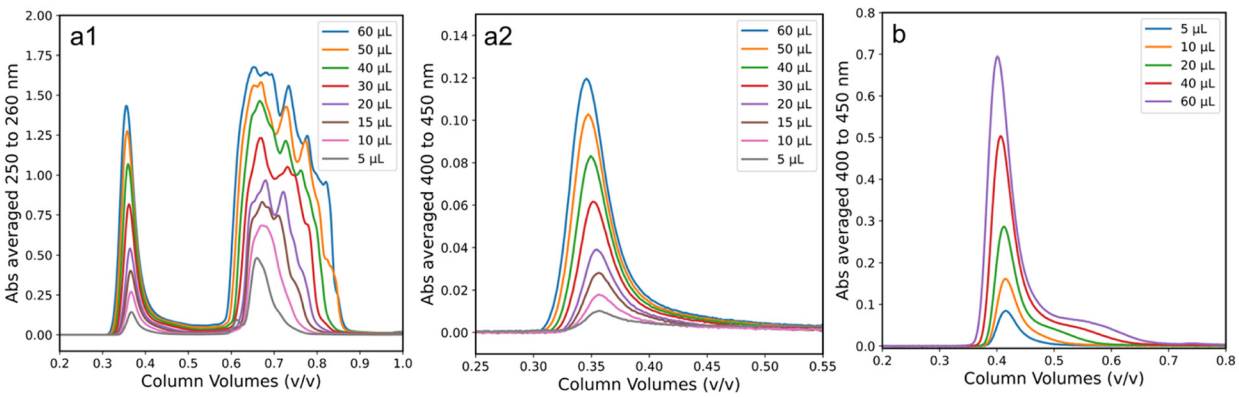


Fig. 4 (a1) Chromatograms of DHNR at various sample loadings from 5 μL to 60 μL (0.25% to 3% c.v.), with column operated at room temperature and flow rates at 20 μL $s^{-1}$. (a2) Chromatogram of the same sample but averaged from 400 to 450 nm, demonstrating similar QD peak shapes at different volumes (b) Chromatogram of CdSe-2.6 at room temperature for various sample loadings, displayed is the average absorbance from 400 to 450 nm.

 

lead to tailing of QD peaks that contributes to reduced purification yield as ligand-shed QD particles can access pores in the silica media and/or attract to the silica media. Ligand-capped QD particles can also attract to the silica media, especially at high QD concentrations.

### Determining purity of SEC *vs.* PR

After establishing the effects of temperature and loading on column performance, the purified QD products were further characterized. Fig. 5a and b show the optical spectra of the QD fraction for CdSe-2.6, plotted with respect to photon wavelength and energy, respectively. In these spectra, the deep UV features show that the eluted QDs are free of optically detectable organic impurities. These QD fractions were collected using the SEC platform, flowing the mobile phase at 20 μL $s^{-1}$ ($\tau$ = 103 s), and collecting the fraction from 0.36 c.v. to 0.48 c.v. NMR analysis of the collected QD fractions were carried out and Fig. 5c shows the results of SEC-purified QDs compared to QDs purified using 1 and 2 rounds of precipitation–redissolution (PR). For this sample, one round of PR is insufficient to remove excess ODE and OA from the reaction mixture, as seen from the presence of ODE peaks at the 4.9 and 5.8 ppm range. On the other hand, one round of SEC at enables rapid ($\tau$ = 103 s) purification of this QD sample to a purity greater than that achieved by 2 rounds of PR. These purified QDs also demonstrate suitability for TEM imaging as shown in Fig. 5d and e.

### Generalizability of SEC platform

After testing small (2.6 nm and 3.5 nm) QDs, the generalizability of this QD purification platform for separation of other QDs with different sizes and shapes was examined. Fig. 6 shows the chromatograms of different QDs including isotropic, anisotropic, and heterostructures. All samples show excellent separation between nanocrystals and dissolved organic molecules at short residence times ($\tau$ = 103 s) as evidenced by the distance between the QD peaks (<0.40 c.v.) and other organic species (<0.55 c.v.), as well as the clear TEM images from the QD-containing fractions. This shows the generalizability of this platform towards rapid separation of QDs with different compositions, sizes, and shapes for QD characterization and imaging.

### Outlook of applications of automated QD purification

This SEC-based platform addresses the challenge of developing a generalized method for QD purification. It enables rapid purification of QDs with minimal effects on QD surface compared to traditional PR methods, while only requiring one single purification step without prior sample preparation besides dilution and filtration. The main strength of this platform lies in its ability to rapidly generate UV-spectra of purified QDs, including the ability to uncover deep-UV features of synthesized QDs if proper UV-transparent solvents (*e.g.*, hexane) are used. Such deep-UV features can help distinguish phases of various QD materials (*e.g.*, zinc blende *vs.* wurtzite phases in II–VI semiconductors), enabling rapid determination of phases without more complex characterization methods (*e.g.*, TEM or XRD).[55]

Besides generating UV spectra of purified QDs, this platform can also rapidly generate samples of high purity QDs at various scales. SEC is a purification method that mostly relies on the difference in accessible volumes between different species and thus can be scaled towards larger preparative scales for rapid purification of QDs for

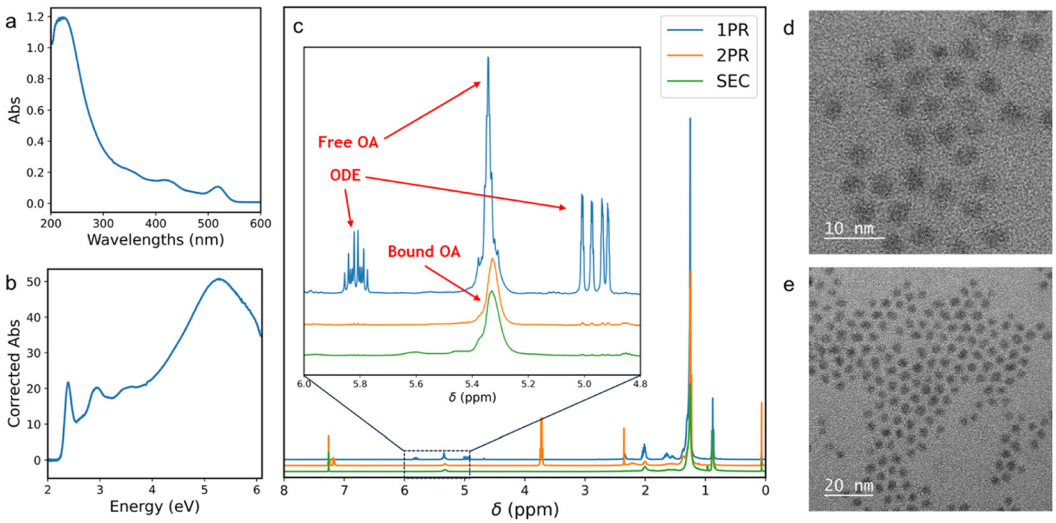


**Fig. 5** Spectra of CdSe-2.6 (2.6 nm) CdSe QDs obtained from the SEC system ($\tau$ = 103 s) in (a) wavelength and (b) energy scales (Jacobian normalized). (c) NMR spectra of purified CdSe-2.6 CdSe QDs obtained from SEC purification compared to precipitation redissolution. PR is unable to remove excess ligands and ODE solvent for small QDs as evident from the peaks in the inset. (d) and (e) TEM micrograph of CdSe-3.5 3.5 nm CdSe QDs purified ($\tau$ = 103 s) using SEC. Approximately 2400 μL of crude sample was purified using 60 runs of 40 μL injections to give 14.4 mL of QDs dispersed in hexanes. Drying of the QD fraction yielded 5 mg of purified QD product that was used for NMR spectroscopy.

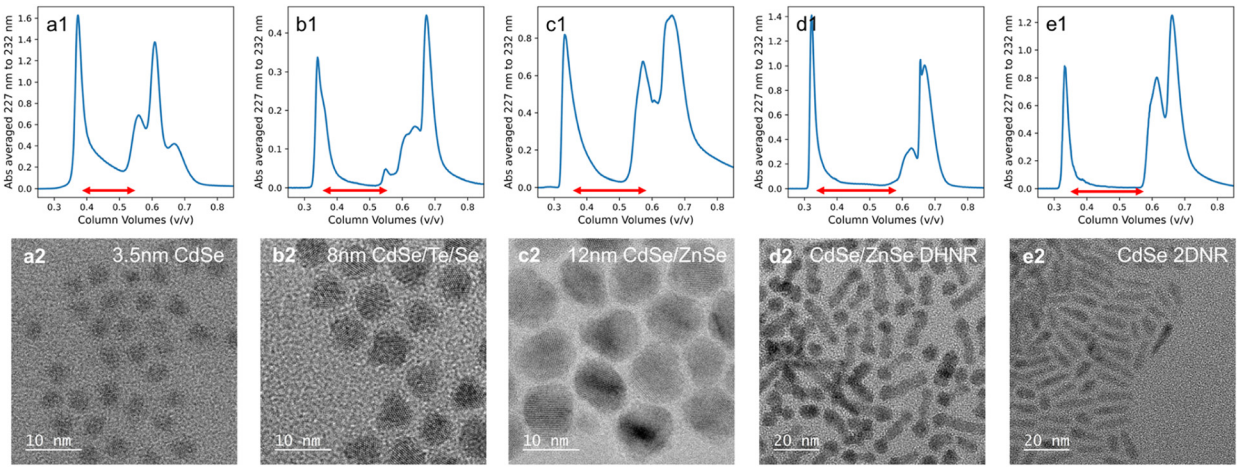


**Fig. 6** Chromatograms (a1–e1) of various QDs of different sizes, shapes, and surface ligands showing good separation between QD and organic peaks, enabling separation of high purity QDs at high yield. TEM micrographs (a2–e2) of respective QDs. All QDs were purified using a column loading of 3% (60 μL) and a flow rate of 20 μL $s^{-1}$ ($\tau$ = 103 s), with 4 c.v. of hexanes used to clean the column before each run. Crude reaction mixtures have a QD concentration of approximately 0.2 wt% to 2 wt% and the purified QD fractions have a quarter the concentration of the crude reaction mixtures. Approximately 10 runs of 60 μL injections were used for each sample to separate about 2400 μL of QDs dispersed in hexanes. This dispersion was then dried at room temperature under a vacuum and redispersed in toluene before being drop-casted on copper TEM grids.

characterization or downstream synthesis and processing (*e.g.*, heterostructure synthesis, device fabrication).[27,28,32,33] TEM imaging of QDs, for instance, requires purified QDs and replacing traditional PR workflows with a more generalized, higher throughput method can help accelerate the synthesis–purification–characterization workflow. Because of the high purity of QD fractions obtained through SEC, various other quantitative characterization methods for analyzing the surface ligands of QDs (quantitative NMR) or composition of QDs (inductively coupled plasma mass spectrometry) can be used to help more comprehensively characterize QDs.

Ligand shedding is a significant phenomenon affecting QD separations using SEC, with the degree of shedding determined by column temperatures and residence times of QDs in the column. Because the column uses rigid silica particles that allow for a wide range of solvents, this SEC-platform can also enable the ligand-exchange of QD particles to prepare QDs with specific surface ligands for various applications.[44] Likewise, because the column can be operated across a range of residence times and temperatures, this platform can also potentially be used as a tool to study the kinetics of ligand-exchange on QD surface in various solvents.

The generalizability of this SEC-based purification approach provides this platform with the ability to be integrated with several existing platforms for QD synthesis. Numerous works have previously described workflows to automate the synthesis and optical characterization of colloidal semiconductor nanostructures to accelerate research in materials discovery.[56–59] However, these automated workflows mostly rely on optical characterization to measure properties of synthesized QDs. Integrating this automated SEC purification platform with automated QD synthesis platforms has the potential to unlock a more comprehensive suite of characterization tools to uncover QD properties such as structure and chemical composition, and perhaps also integrate these automated synthesis platforms to other platforms (*e.g.*, automated spin coating) to test the performance of synthesized QDs for downstream applications.

## Conclusions

In this work, we demonstrated a small (2 mL) scale automated SEC purification platform suitable for purification of QDs from nonpolar organic phases, using commercially available fully porous silica columns and microfluidic flow control hardware. Silica columns allow for facile separation of QDs directly from crude reaction mixtures using a range of different solvents. They can also handle high flow rates and a range of temperatures, enabling a rapid, generalizable QD purification workflow compared to established precipitation–redissolution based QD purification methods.

We successfully demonstrated SEC-based purification of various QDs samples on Nucleosil 100 Å silica and explored the influence of various column operating parameters (flow rate, temperature, column loading) on separation performance. Separation of small (3.5 nm) QDs revealed mass transfer limitations at high flow rate leading to peak broadening, while low flow rates and high temperatures lead to ligand stripping from QD particles and peak tailing. The column demonstrates high loading capacity up to 3% c.v., but higher concentrations of QDs will lead to peak tailing at higher column loadings due to interaction between QD particles and the column stationary phase. These experiments highlight the ability to tune the ligand coverage of QD fractions by varying column parameters of temperature and flow rates.

Overall, the SEC platform demonstrates the ability for rapid (80 s) purification of QDs at high column loadings for QDs of various shapes and sizes in nonpolar organic mixtures. QD fractions from this column show high purity when compared to

 

QDs purified using the traditional precipitation–dissolution method, based on $^{1}$H NMR analysis of purified QDs. This platform not only enables the acceleration of the synthesis–purification–characterization workflow in QD discovery and optimization research but also opens the possibility of potential integration with existing automated experimental workflows to enable more comprehensive characterization.

## Author contributions

Conceptualization: P. J. A. K. and R. H. J. X. designed, automated, and operated the SEC platform, while C. H., Y. D., and L. P. K. provided the various QD samples as well as advised on the choice of column stationary and mobile phases and the various characterization methods. Funding acquisition: P. J. A. K. and M. S. All authors wrote, revised, and reviewed the manuscript.

## Conflicts of interest

There are no conflicts to declare.

## Data availability

Supplementary information is available. See DOI: https://doi.org/10.1039/d5re00302d. Detailed information for the preparation of the various QD samples used in this work, operation of the SEC platform, and platform schematics are listed in the supplementary information. Python code for automated operation of the hardware is shared publicly on the following GitHub repository: https://github.com/AutonomousWorkflows/SEC_Automation.

## Acknowledgements

The authors acknowledge financial support from the Grainger College of Engineering under the Strategic Research Initiative for conducting the research reported in this work. We also thank Dr. Andrew B. Greytak and Md Moinul Islam from the University of South Carolina for invaluable advice on implementation of SEC-based techniques for QD separation.

## References

1 B. A. Kairdolf, A. M. Smith, T. H. Stokes, M. D. Wang, A. N. Young and S. Nie, *Annu. Rev. Anal. Chem.*, 2013, **6**, 143–162.
2 J. Li and J.-J. Zhu, *Analyst*, 2013, **138**, 2506–2515.
3 E. A. Weiss, *ACS Energy Lett.*, 2017, **2**, 1005–1013.
4 P. Sun, Z. Xing, Z. Li and W. Zhou, *Chem. Eng. J.*, 2023, **458**, 141399.
5 H. Liu, M. Li, O. Voznyy, L. Hu, Q. Fu, D. Zhou, Z. Xia, E. H. Sargent and J. Tang, *Adv. Mater.*, 2014, **26**, 2718–2724.
6 A. De Iacovo, F. Mitri, S. De Santis, C. Giansante and L. Colace, *ACS Sens.*, 2024, **9**, 555–576.
7 H. Hosokawa, R. Tamaki, T. Sawada, A. Okonogi, H. Sato, Y. Ogomi, S. Hayase, Y. Okada and T. Yano, *Nat. Commun.*, 2019, **10**, 43.
8 P. R. Brown, D. Kim, R. R. Lunt, N. Zhao, M. G. Bawendi, J. C. Grossman and V. Bulović, *ACS Nano*, 2014, **8**, 5863–5872.
9 C. M. Cirloganu, L. A. Padilha, Q. Lin, N. S. Makarov, K. A. Velizhanin, H. Luo, I. Robel, J. M. Pietryga and V. I. Klimov, *Nat. Commun.*, 2014, **5**, 4148.
10 V. I. Klimov, T. A. Baker, J. Lim, K. A. Velizhanin and H. McDaniel, *ACS Photonics*, 2016, **3**, 1138–1148.
11 F. Purcell-Milton and Y. K. Gun'ko, *J. Mater. Chem.*, 2012, **22**, 16687–16697.
12 J. Yang, M. K. Choi, U. J. Yang, S. Y. Kim, Y. S. Kim, J. H. Kim, D.-H. Kim and T. Hyeon, *Nano Lett.*, 2021, **21**, 26–33.
13 K. Bourzac, *Nature*, 2013, **493**, 283.
14 X. Dai, Y. Deng, X. Peng and Y. Jin, *Adv. Mater.*, 2017, **29**, 1607022.
15 F. P. García de Arquer, D. V. Talapin, V. I. Klimov, Y. Arakawa, M. Bayer and E. H. Sargent, *Science*, 2021, **373**, 6555.
16 Y. Shirasaki, G. J. Supran, M. G. Bawendi and V. Bulović, *Nat. Photonics*, 2013, **7**, 13–23.
17 E. Jang and H. Jang, *Chem. Rev.*, 2023, **123**, 4663–4692.
18 Y.-S. Park, J. Roh, B. T. Diroll, R. D. Schaller and V. I. Klimov, *Nat. Rev. Mater.*, 2021, **6**, 382–401.
19 N. Ahn, C. Livache, V. Pinchetti, H. Jung, H. Jin, D. Hahm, Y.-S. Park and V. I. Klimov, *Nature*, 2023, **617**, 79–85.
20 L. Carbone, C. Nobile, M. De Giorgi, F. Della Sala, G. Morello, P. Pompa, M. Hytch, E. Snoeck, A. Fiore, I. R. Franchini, M. Nadasan, A. F. Silvestre, L. Chiodo, S. Kudera, R. Cingolani, R. Krahne and L. Manna, *Nano Lett.*, 2007, **7**, 2942–2950.
21 O. Chen, J. Zhao, V. P. Chauhan, J. Cui, C. Wong, D. K. Harris, H. Wei, H.-S. Han, D. Fukumura, R. K. Jain and M. G. Bawendi, *Nat. Mater.*, 2013, **12**, 445–451.
22 D. Jung, J. W. Park, S. Min, H. J. Lee, J. S. Park, G.-M. Kim, D. Shin, S. Im, J. Lim, K. H. Kim, J. A. Chae, D. C. Lee, R. Pugin, X. Bulliard, E. Hwang, J.-S. Park, Y.-S. Park and W. K. Bae, *Nat. Commun.*, 2024, **15**, 5561.
23 B. Chen, W. Zheng, F. Chun, X. Xu, Q. Zhao and F. Wang, *Chem. Soc. Rev.*, 2023, **52**, 8374–8409.
24 G. W. Huang, C. Y. Chen, K. C. Wu, M. O. Ahmed and P. T. Chou, *J. Cryst. Growth*, 2004, **265**, 250–259.
25 S. B. Brichkin and V. F. Razumov, *Russ. Chem. Rev.*, 2016, **85**, 1297.
26 Y. Yang, J. Li, L. Lin and X. Peng, *Nano Res.*, 2015, **8**, 3353–3364.
27 E. Dhaene, J. Billet, E. Bennett, I. Van Driessche and J. De Roo, *Nano Lett.*, 2019, **19**, 7411–7417.
28 E. Drijvers, J. De Roo, P. Geiregat, K. Fehér, Z. Hens and T. Aubert, *Chem. Mater.*, 2016, **28**, 7311–7323.
29 Y. Shen, M. Y. Gee and A. B. Greytak, *Chem. Commun.*, 2017, **53**, 827–841.
30 H. Xu, J. Song, P. Zhou, Y. Song, J. Xu, H. Shen, S. Fang, Y. Gao, Z. Zuo, J. M. Pina, O. Voznyy, C. Yang, Y. Hu, J. Li, J. Du, E. H. Sargent and F. Fan, *Nat. Photonics*, 2024, **18**, 186–191.
31 Y. Liu, N. Peard and J. C. Grossman, *J. Phys. Chem. Lett.*, 2019, **10**, 3756–3762.

32 Y. Shen, M. Y. Gee, R. Tan, P. J. Pellechia and A. B. Greytak, *Chem. Mater.*, 2013, **25**, 2838–2848.
33 R. Tan, Y. Shen, S. K. Roberts, M. Y. Gee, D. A. Blom and A. B. Greytak, *Chem. Mater.*, 2015, **27**, 7468–7480.
34 P. Paydary and P. Larese-Casanova, *Int. J. Environ. Anal. Chem.*, 2015, **95**, 1450–1470.
35 S. T. Skowron, T. W. Chamberlain, J. Biskupek, U. Kaiser, E. Besley and A. N. Khlobystov, *Acc. Chem. Res.*, 2017, **50**, 1797–1807.
36 A. Botman, J. J. L. Mulders and C. W. Hagen, *Nanotechnology*, 2009, **20**, 372001.
37 T. Kim, M. L. Kelley, D. Kim, A. B. Greytak and S. Jeong, *Int. J. Precis. Eng. Manuf. - Green Technol.*, 2021, **8**, 1309–1321.
38 L. A. King and D. J. Riley, *J. Phys. Chem. C*, 2012, **116**, 3349–3355.
39 A. J. Morris-Cohen, M. D. Donakowski, K. E. Knowles and E. A. Weiss, *J. Phys. Chem. C*, 2010, **114**, 897–906.
40 B. Shakeri and R. W. Meulenberg, *Langmuir*, 2015, **31**, 13433–13440.
41 J. Wang, X. Huang, L. Ruan, T. Lan and J. Ren, *Electrophoresis*, 2013, **34**, 1764–1771.
42 J.-K. Wu, Z.-Q. Tian, Z.-L. Zhang, A.-A. Liu, B. Tang, L.-J. Zhang, Z.-L. Chen and D.-W. Pang, *Talanta*, 2016, **159**, 64–73.
43 D. Chen, Y. Yuan, J. Yu, D. T. Chiu and C. Wu, *Anal. Chem.*, 2018, **90**, 5569–5575.
44 Y. Shen, A. Roberge, R. Tan, M. Y. Gee, D. C. Gary, Y. Huang, D. A. Blom, B. C. Benicewicz, B. M. Cossairt and A. B. Greytak, *Chem. Sci.*, 2016, **7**, 5671–5679.
45 L. Pitkänen and A. M. Striegel, *TrAC, Trends Anal. Chem.*, 2016, **80**, 311–320.
46 T. Arita, T. Yoshimura and T. Adschiri, *Nanoscale*, 2010, **2**, 1467–1473.
47 L. Alamo-Nole, S. Bailon-Ruiz, O. Perales-Perez and F. R. Roman, *Anal. Methods*, 2012, **4**, 3127–3132.
48 M. Wang, G. R. Bardajee, S. Kumar, M. Nitz, G. D. Scholes and M. A. Winnik, *J. Chromatogr. A*, 2009, **1216**, 5011–5019.
49 A. Roberge, J. H. Dunlap, F. Ahmed and A. B. Greytak, *Chem. Mater.*, 2020, **32**, 6588–6594.
50 A. Roberge, J. L. Stein, Y. Shen, B. M. Cossairt and A. B. Greytak, *J. Phys. Chem. Lett.*, 2017, **8**, 4055–4060.
51 F. Ahmed, M. L. Kelley, M. V. S. Chandrashekhar and A. B. Greytak, *J. Phys. Chem. C*, 2021, **125**, 17796–17805.
52 P. Hong, S. Koza and E. S. P. Bouvier, *J. Liq. Chromatogr. Relat. Technol.*, 2012, **35**, 2923–2950.
53 H. G. Barth, C. Jackson and B. E. Boyes, *Anal. Chem.*, 1994, **66**, 595–620.
54 P. L. Dubin, *Aqueous size-exclusion chromatography*, Elsevier, 1988, vol. 40.
55 S. J. Lim, A. Schleife and A. M. Smith, *Nat. Commun.*, 2017, **8**, 14849.
56 A. Vikram, K. Brudnak, A. Zahid, M. Shim and P. J. A. Kenis, *Nanoscale*, 2021, **13**, 17028–17039.
57 R. H. J. Xu, L. P. Keating, A. Vikram, M. Shim and P. J. A. Kenis, *Chem. Mater.*, 2024, **36**, 1513–1525.
58 R. W. Epps, M. S. Bowen, A. A. Volk, K. Abdel-Latif, S. Han, K. G. Reyes, A. Amassian and M. Abolhasani, *Adv. Mater.*, 2020, **32**, 1–9.
59 S. Li, R. W. Baker, I. Lignos, Z. Yang, S. Stavrakis, P. D. Howes and A. J. Demello, *Mol. Syst. Des. Eng.*, 2020, **5**, 1118–1130.
60 L. P. Keating, C. Huang and M. Shim, *Rev. Sci. Instrum.*, 2024, **95**, 63704.
61 C. Huang, Y. Jiang, G. A. Drake, L. P. Keating and M. Shim, *J. Chem. Phys.*, 2023, **158**, 24.
62 G. A. Drake, L. P. Keating, C. Huang and M. Shim, *J. Am. Chem. Soc.*, 2024, **146**, 9074–9083.